Virtual Heart Models Help Elucidate the Role of Border Zone in Sustained Monomorphic Ventricular Tachycardia

Eduardo Castañeda[1,2(✉)], Masahito Suzuki[3], Hiroshi Ashikaga[4], Èric Lluch[2], Felix Meister[2], Viorel Mihalef[5], Chloé Audigier[6], Andreas Maier[1], Henry Halperin[7], and Tiziano Passerini[5]

[1] Pattern Recognition Lab, Department of Computer Science, Friedrich-Alexander University Erlangen-Nürnberg, Erlangen, Germany
eduardo.castaneda@fau.de
[2] Siemens Healthineers, Digital Technologies and Innovation, Erlangen, Germany
[3] JA Toride Medical Ctr, Department of Cardiology, Ibaraki, Japan
[4] Pali Momi Heart Center, Aiea, Hawaii, USA
[5] Siemens Healthineers, Digital Technologies and Innovation, Princeton, USA
[6] Advanced Clinical Imaging Technology, Siemens Healthcare, Lausanne, Switzerland
[7] Johns Hopkins University, Department of Medicine, Division of Cardiology, Baltimore, Maryland, USA

Abstract. Post-ischemic Ventricular Tachycardia (VT) is sustained by a depolarization wave re-entry through channel-like structures within the post-ischemic scar. These structures are usually formed by partially viable tissue, called Border Zone (BZ). Understanding the anatomical and electrical properties of the BZ is crucial to guide ablation therapy to the right targets, reducing the likelihood of VT recurrence. Virtual Heart methods can provide ablation guidance non-invasively, but they have high computational complexity and have shown limited capability to accurately reproduce the specific mechanisms responsible for clinically observed VT. These outstanding challenges undermine the utility of Virtual Hearts for high precision ablation guidance in clinical practice. In this work, fast phenomenological models are developed to efficiently and accurately simulate the re-entrant dynamics of VT as observed in 12-lead ECG. Two porcine models of Myocardial Infarction (MI) are used to generate personalized bi-ventricular models from pre-operative LGE-MRI images. Myocardial conductivity and action potential duration are estimated using sinus rhythm ECG measurements. Multiple hypotheses for the BZ tissue properties are tested, and optimal values are identified. These allow the Virtual Heart model to produce VTs with good agreements with measurements in terms of ECG lead polarity and VT cycle length. Efficient GPU implementation of the cardiac electrophysiology model allows computation of sustained monomorphic VT in times compatible with the clinical workflow.

Supplementary Information The online version contains supplementary material available at https://doi.org/10.1007/978-3-031-43990-2_21.

H. Greenspan et al. (Eds.): MICCAI 2023, LNCS 14226, pp. 216–225, 2023.
https://doi.org/10.1007/978-3-031-43990-2_21

Keywords: Cardiac modeling · VT · VAAT · ECG simulation

1 Introduction

Post-ischemic Ventricular Tachycardia (VT) is an arrhythmia that occurs after a myocardial infarction event. During Myocardial Infarction (MI), the blood flow to an area of the heart is blocked, producing tissue death and scarring [8]. After tissue healing, partially viable areas can appear within the scar tissue. These areas, usually referred to as Border Zone (BZ), contain a complex mixture of scar and viable myocardium [8]. These can produce channel-like structures that act as paths for an abnormal depolarization wave re-entry that sustains the VT [8,22].

Catheter ablation is recommended for ischemic heart disease patients, in the presence of recurrent monomorphic VT despite anti-arrhythmic drug therapy. Ablation therapy aims at destroying a part of the re-entry path (channel) that sustains the VT [22]. Precise identification of the target for ablation is paramount to maximize the efficacy of the procedure in terms of reduction of VT recurrence, while minimizing the amount and extension of ablation lesions. Both intracardiac electrograms and pre-operative Late Gadolinium Enhanced MRI have been adopted for channel identification [25], however the rate of success of catheter ablation is still unsatisfactory [22,25].

Virtual-Heart Arrhythmia Ablation Targeting (VAAT) methods have been developed to improve the utility of pre-operative imaging by using image-based computational models to reproduce the patient-specific re-entrant dynamics of the arrhythmia and thus increase precision in the localization of ablation targets [2,9,25]. These approaches generally suffer from two limitations. On the one hand, they have not shown the capability to consistently reproduce the same re-entries observed in-vivo and as measured by 12-lead ECG. On the other hand, they require a laborious process and time-intensive simulations incompatible with clinical use.

In this paper, we present a validation study of a novel VAAT method based on efficient phenomenological models of electrophysiology for high-fidelity simulation of VT. We successfully reproduce the inducibility of sustained monomorphic VT (more than 30 s) in two animal models of scar-related VT. In addition, we reproduce the ECG signature of each measured VT circuit, in terms of the polarity in the QRS complex of each lead as well as the VT cycle length. Finally, we demonstrate the feasibility of using this method in clinical practice by showing considerable speed up compared to the state-of-the art.

2 Methods

2.1 Data Description

Two porcine models of MI [11] were used for this study. The animal study was reviewed and approved by the Johns Hopkins University Animal Care and Use

Committee (Baltimore, MD). High-resolution LGE-MRI (Aera, Siemens Healthineers) images of the subjects were acquired 6 weeks after the MI induction procedure. One week after, the swine underwent the VT ablation procedure. During the procedure, one VT was successfully induced in case 1, and three different VTs were induced in case 2. The 12-lead ECG (CardioLab, GE Healthcare) was acquired pre-operatively and during VT for both cases. The QRS and QT duration in the ECGs measured during sinus rhythm were annotated by an electrophysiologist. Additionally, the ECG VT morphology was reviewed by an electrophysiologist, which determined the VT cycle length and estimated the approximate exit site location using the ECG lead polarity [1].

2.2 Anatomical Model Generation

The right ventricular (RV) endocardium, left ventricular (LV) endocardium, and LV epicardium were manually contoured and reviewed by an electrophysiologist. The computational domain for the electrophysiology model was defined as a Cartesian grid of isotropic 0.5 mm resolution, obtained by rasterization of the segmented surfaces [18]. A rule-based model of the myocardial fibers was also included [3]. The complete anatomical generation process was applied as previously described [26]. A generic swine torso model was manually deformed and oriented to fit the scout MRI images of each subject.

The scar and BZ were semi-automatically segmented by an expert and validated by an electrophysiologist. The full-width half-maximum method [23] was applied to the stack of LGE-MRI images after resampling to an isotropic 3D grid of 0.4 mm. The BZ segmentation was constrained to be within a maximum distance of 4 mm from the closest scar following the assumption that BZ tissue closely surrounds the scar core [23], which was consistent with measured voltage maps. The tissue segmentation was then post-processed. First, we applied morphological closing with a spherical kernel of 4 voxel radius to close small holes of BZ within the scar. Then we applied morphological opening with a spherical kernel of 1 voxel radius to remove small and isolated scar patches. Lastly, we applied a dilation (max 2 mm) of the scar and BZ tissues in the transmural direction to preserve transmurality after the domain rasterization. Preserving scar transmurality prevents the generation of spurious endocardial or epicardial re-entry pathways inconsistent with evidence from LGE-MRI and voltage maps. See the Supplementary Materials for more details about the implementation.

2.3 Electrophysiology Simulation

The electrophysiology model is based on the monodomain equation using the modified Mitchell-Schaeffer cellular model [6,19]. The numerical solver is an efficient GPU implementation of the Lattice Boltzmann Method [17,21]. The time-varying extracellular potential on the animal torso is computed following the Boundary Element Method (BME) [26]. Virtual electrodes were placed on the animal torso in the locations used in the clinical study, which were validated by

an electrophysiologist, and virtual 12-lead ECG signals were derived [17]. Each individual lead signal amplitude is then normalized to mitigate uncertainty on the torso anatomy.

Scar tissue was modeled as a non-conductive material. The BZ tissue was modeled as conductive, isotropic, and with a longer Action Potential Duration (APD) than the healthy tissue [16]. The transversal Conduction Velocity (CV) in the healthy myocardium was set to 0.45 times the longitudinal CV [7].

To reproduce the fast conduction produced by the Purkinje network, a Fast Endocardial Conductive (FEC) layer of 3 mm was added to the model to account for the increased transmurality of Purkinje networks in porcine models [24]. Longitudinal CV was set 4 times higher than in the healthy myocardium, while the transversal CV was unchanged [7,14]. The FEC layer was not placed over scar or BZ areas, which were measured as non-conductive by voltage mapping during the ablation procedure.

2.4 Parameter Personalization

The model parameters were tuned to match the ECG measurements during sinus rhythm. To simulate sinus rhythm, a one-second-long simulation was run with four pacing points placed in the basal and apical areas of the LV and RV septal walls to produce depolarization patterns consistent with previously published observations [10]. A grid-search approach was used to optimize the myocardial diffusivity and the closing time constant of the current gate (τ_{close}) of the Mitchell and Schaeffer cellular model, to match the measured QRS and QT interval respectively.

Myocardial diffusivity was sampled in a range of values corresponding to CV between 0.4 and 0.75 m/s, with 0.01 m/s steps, consistent with previous approaches [7,14]. After adjusting the CV, the τ_{close} parameter was sampled in a range of values corresponding to myocardial APD between 0.14 and 0.3 s with 0.005 s steps, consistent with reported values [13]. The APD was defined as the amount of time with voltage higher than 20% of its maximum value for each experiment.

The reference QRS and QT duration in the measured ECGs were annotated by an electrophysiologist in a digital trace plotted with a paper speed of 50 mm/s. The QRS and QT duration in the simulated ECGs were visually annotated by an expert and the set of parameters leading to the best match with the measured ECG were validated by an electrophysiologist. Due to the infarction features present in the ECG, such as ST elevation [12], the measurement procedure and thus the optimization procedure could not be fully automated, since automatic extraction of QRS and QT duration led to a relatively large uncertainty margin of up to 20 ms depending on the selected ECG lead and signal morphology.

Electrophysiology properties of the BZ were not personalized based on sinus rhythm ECG measurements, since we observed minimal effect on simulated sinus rhythm QRS and QT duration from variations of the BZ parameters within the range of previously reported values [7].

2.5 VT Induction Procedure

The simulation of a programmed stimulation experiment included three phases: model preconditioning, artificial stimulation delivery, and spontaneous activity simulation. First, the internal states of the model were pre-conditioned by simulating 5 s of sinus rhythm at 60 bpm. Then, 8 stimuli were delivered at a constant period S1, which ranged between 0.3 and 0.6 s, followed by three extra stimuli delivered with delays S2, S3, and S4. The pacing times S2, S3, and S4 were automatically reduced until VT was induced or no activation was produced, following the procedure described in the Supplementary Materials. The stimuli were delivered from one point at a time, which could be located in the RV outflow tract, RV apex, or each AHA region barycenter. Other points in proximity to areas that were visually identified as possible re-entry channels were additionally tested. For efficiency purposes, the internal states of the simulation were saved after the preconditioning phase and after the S1 stimuli train and were re-used for later simulations.

To elucidate the role of Electrophysiological (EP) properties of the BZ on the generation and maintenance of VT, multiple programmed stimulation experiments were conducted with varying BZ parameters. BZ diffusivity was sampled in a range of values corresponding to CV between 0.14 and 0.23 m/s, with 0.01 m/s steps, consistent with previous approaches [5,16]. BZ APD was increased from 0.015 s to 0.06 s over the myocardial APD with 0.015 s steps, consistent with reported values [5,16].

All simulations were performed on a high-performance GPU cluster with 24 GPUs (Tesla-V100-SXM2, NVIDIA Corporation) scheduled to perform multiple experiments in parallel. Additionally, to save computation time, the simulations were stopped 1 s after the last delivered stimulus if no spontaneous activity was present. If spontaneous activation was present, the simulations were computed for a maximum of 30 s after the last delivered stimulus. Each simulation was classified as inducible with sustained activity if the spontaneous activity lasted for 30 s after the last stimulus. For these simulations, the pseudo-ECG was computed and the intracardiac potentials sampled in each of the AHA region barycenters were saved for later analysis.

2.6 Analysis of VT Inducibility

The intracardiac potentials of each inducible simulation were analyzed by calculating the Cycle Length (CL) of spontaneous activity using a moving window of 4 s. The mean and standard deviation time between Action Potential (AP) peaks in the moving window was computed. This was done to study the evolution of the sustained VT during its duration. Additionally, this allowed us to determine whether the VT was monomorphic, in which case CL standard deviation is minimized.

3 Results

3.1 Personalization Results

The personalization resulted in a myocardial CV of 0.68 m/s and 0.64 m/s, which produced a QRSd consistent with the measurements of 70 ms and 80 ms, for case 1 and 2 respectively. The personalized APDs of 0.155 s for both cases produced a QTd of 370 ms and 380 ms for case 1 and case 2 respectively, which were in accordance with the measurements. The personalization was done with a BZ CV of 0.23 m/s and an APD increase of 0.03 s for both cases.

3.2 Inducibility of VT

The personalized values obtained in Sect. 3.1 were used for the VT inducibility simulations following the protocol described in Sect. 2.4.

For case 1, the artificial stimulation was delivered from 3 points as tested in the clinical scenario: the RV apex, AHA regions 1 and 2. An additional point in the LV apex was placed near a visually identified channel. A total of 7050 virtual programmed stimulation experiments were performed with an average compute time of 5 h and 31 min per GPU, resulting in 201 induced VTs. All VTs shared the same ECG signature, and were induced after LV apex pacing. The ECG signature was consistent with that of the measured VT. Additionally, one parameter combination produced VT with the same CL as the measured VT (0.27 s). This was achieved with a BZ CV of 0.21 m/s and BZ APD of 0.17 s. The 12-lead-ECG polarity matched in all leads. A qualitative comparison is shown in Fig. 1a. After inspection of the computed time-dependent transmembrane potential field (movie included in the Supplementary Materials), it was determined that the VT was a result of a re-entry through an LV apex channel. This was consistent with the measurements as confirmed by an electrophysiologist.

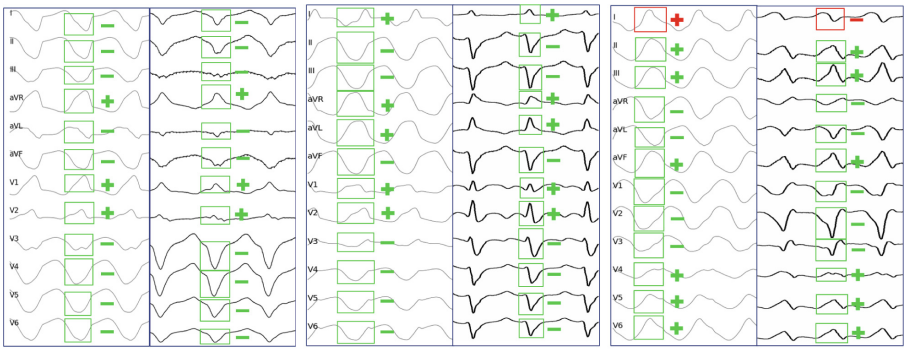

(a) Case 1 VT 1 (b) Case 2 VT 1 (c) Case 2 VT 2

Fig. 1. Computed VT morphology (left) vs. Measured VT morphology (right) for both cases.

For case 2, the artificial pacing was delivered from the RV outflow tract, RV Apex, and LV apex. Additionally, AHA regions 17, 15, 9, 8, 7, which surrounded the scar and BZ tissue were also tested. An extra point was placed inside the BZ tissue in the RV septum. Due to the more extensive BZ area and low CL of the measured VTs in this case, a larger span of parameter values for the BZ diffusivity was tested, corresponding to BZ CVs in the range [0.14, 0.32] m/s. In this case, 26646 inducibility experiments were done with an average computation time of 27 h and 39 min per GPU. 2414 experiments produced sustained monomorphic VT, with 4 distinct ECG signatures. Two of these ECG signatures were identified in VTs sustained by a LV apical re-entry pathway, and 2 in VTs sustained by a RV septal re-entry pathway. Both re-entry pathways are consistent with two of the VT exit sites estimated based on measured VT ECG. For these cases, one parameter combination produced optimal match between computed and measured VTs, in terms of CL and ECG lead polarity. This was achieved with BZ CV of 0.324 s and BZ APD of 0.1725 s. The best matching computed VT with LV apical exit site (VT 1) had a CL of 0.257 s (measured 0.240 s), and same lead polarity as the measured ECG. The best matching VT with RV septal exit site (VT 2) had a CL of 0.261 s (measured 0.190 s) and lead polarity consistent with the measured ECG except lead I. The qualitative comparison between the results can be observed in Figs. 1b and 1c. The re-entry movies for these cases can be found in the Supplementary Materials. The clinical agreement in both VTs was confirmed by an electrophysiologist.

3.3 Comparison with Previous Modeling Approaches

The modeling configuration reported by Mendonca Costa et al. [7] was reproduced in our study for Case 1. A FEC layer of 0.5 mm was placed in the endocardial layer, also covering BZ and Scar tissue. The FEC layer was configured with a longitudinal CV 6 times the healthy myocardial longitudinal CV, while the transversal CV was set equal. In the endocardium over the scar and BZ tissue the isotropic CV was set to 6 times the BZ CV. Our personalization approach was tested with this configuration, but we could not match the sinus rhythm QRSd with the largest considered myocardial CV of 0.75 m/s. The inducibility tests were repeated for this configuration using the baseline parameters reported by Mendonca-Costa et al. No sustained inducibility was achieved in this case.

4 Discussion

In this manuscript, a pipeline and methodology to simulate monomorphic VT re-entrant dynamics was described. This method utilized fast and computationally efficient methods to solve the monodomain equation for cardiac electrophysiology, and phenomenological models for the cellular AP description. The results of this paper show that this approach allows to match clinical measurements of monomorphic VT, matching both the cycle length and ECG lead polarity, after myocardial parameter personalization and BZ parameter exploration. The

optimal BZ tissue properties, maximizing the agreement between simulated and measured VT, could not be identified based on commonly adopted modeling assumptions (e.g. as a pre-defined ratio of myocardial tissue properties). Instead, we observed significant case-by-case variability, suggesting that improved methods for estimation of BZ properties are necessary to increase fidelity of Virtual Heart models for monomorphic VT simulation. Although this was only validated in 2 cases, we plan to add more in the continuation of the project. To our knowledge, this is the largest validation study of Virtual Heart models focusing on VT ECG. Lopez Perez et al. performed a similar study only using one case, showing a good agreement of VT morphology but not CL matching [15].

Our results show that BZ parameter exploration is necessary to reproduce the clinical VT. Accurately determining BZ tissue properties in a prospective setting, when VT ECG measurements are not available, requires future investigation. We hypothesize that it is possible to identify BZ features in sinus rhythm ECG measurements, possibly using more complex signal features than QRS and QT duration, although this has not been investigated in our study.

Additionally, we reproduced the alternative modeling approach described by Mendonca Costa et al. [7]. This approach showed a sub-optimal match of sinus rhythm ECG measurements. VT inducibility testing resulted in no sustained activity for the case considered in this study. We hypothesize that the lack of VT inducibility is related to incorrect selection of the BZ properties, and also to the assumption of a FEC covering the endocardial scar. This could produce spurious sub-endocardial re-entry pathways, preventing the maintenance of wave re-entry. Modeling assumptions can have a significant impact on the fidelity of the results, so it is important to evaluate them individually in the context of the available observations from each specific case.

The proposed pipeline is potentially capable of delivering results with times compatible with clinical practice: for a given parameter combination, a virtual programmed stimulation experiment requires 20 min of computation on a single GPU (i.e. 41 s per simulated second). This is faster than other approaches: 1 h per simulated second [20], or 17 min per simulated second (VARP) [4]. Nonetheless, absent a definitive way to characterize BZ parameters, the grid search requires extensive computational efforts, limiting direct application in a clinical setting. Other methods can identify plausible re-entry circuits in almost real-time using simplified electrophysiology models [4]. In contrast, our work focuses on identifying the circuits of clinical relevance, with the goal of proposing the minimal set of ablation targets with the maximal efficacy.

Clinical applicability will also require the full automation of several steps of this pipeline, including the tissue segmentation, parameter personalization, and unique VT signature characterization. At the current stage of our research, we have focused on careful manual curation of the input data to help reduce the potential impact of uncertainty due to data quality or algorithm performance.

An additional limitation of this study is that the virtual ECG model is not able to produce the full range of ECG morphologies observed in measured signals, in particular high frequency features in ECG leads including changes in

slope, narrowing and notches within the QRS complex, as observed in Figs. 1a, 1b, and 1c. These signal characteristics might be produced by tissue properties heterogeneity which we do not include in our model. Nonetheless, the good agreement achieved in lead polarity suggests that the simulated re-entrant VTs follows a similar re-entry pathway as the corresponding measured VT.

The Virtual Heart model was not capable to match all measured VTs in case 2 in this study, characterized by a comparatively larger infarct extent, suggesting that additional VT exit sites may have been manifest in vivo, while not being produced in the model. As observed in previous computational modeling studies, we still have an incomplete understanding of the role of uncertainty on scar and BZ extent, as determined by the image processing and segmentation pipeline, on the model fidelity. This is a limitation of the current study to be addressed with larger validation studies including a wide variety of infarction presentations in pre-operative imaging.

Acknowledgements. The animal study was reviewed and approved by the Johns Hopkins University Animal Care and Use Committee (Baltimore, MD). Animal Welfare Assurance Number A3272-01.

References

1. Andreu, D., et al.: A QRS axis-based algorithm to identify the origin of scar-related ventricular tachycardia in the 17-segment American Heart Association model. Heart Rhythm **15**(10), 1491–1497 (2018)
2. Ashikaga, H., et al.: Feasibility of image-based simulation to estimate ablation target in human ventricular arrhythmia. Heart Rhythm **10**(8), 1109–1116 (2013)
3. Bayer, J.D., Blake, R.C., Plank, G., Trayanova, N.A.: A novel rule-based algorithm for assigning myocardial fiber orientation to computational heart models. Ann. Biomed. Eng. **40**, 2243–2254 (2012)
4. Campos, F.O., et al.: An automated near-real time computational method for induction and treatment of scar-related ventricular tachycardias. Med. Image Anal. **80**, 102483 (2022)
5. Campos, F.O., et al.: Factors promoting conduction slowing as substrates for block and reentry in infarcted hearts. Biophys. J. **117**(12), 2361–2374 (2019)
6. Corrado, C., Niederer, S.A.: A two-variable model robust to pacemaker behaviour for the dynamics of the cardiac action potential. Math. Biosci. **281**, 46–54 (2016)
7. Costa, C.M., et al.: Determining anatomical and electrophysiological detail requirements for computational ventricular models of porcine myocardial infarction. Comput. Biol. Med. **141**, 105061 (2022)
8. De Bakker, J., et al.: Reentry as a cause of ventricular tachycardia in patients with chronic ischemic heart disease: electrophysiologic and anatomic correlation. Circulation **77**(3), 589–606 (1988)
9. Deng, D., Prakosa, A., Shade, J., Nikolov, P., Trayanova, N.A.: Sensitivity of ablation targets prediction to electrophysiological parameter variability in image-based computational models of ventricular tachycardia in post-infarction patients. Front. Physiol. **10**, 628 (2019)
10. Durrer, D., Van Dam, R.T., Freud, G., Janse, M., Meijler, F., Arzbaecher, R.: Total excitation of the isolated human heart. Circulation **41**(6), 899–912 (1970)

11. Estner, H.L., et al.: The critical isthmus sites of ischemic ventricular tachycardia are in zones of tissue heterogeneity, visualized by magnetic resonance imaging. Heart Rhythm **8**(12), 1942–1949 (2011)
12. Gard, J.J., Bader, W., Enriquez-Sarano, M., Frye, R.L., Michelena, H.I.: Uncommon cause of ST elevation. Circulation **123**(9), e259–e261 (2011)
13. Kong, W., Fakhari, N., Sharifov, O.F., Ideker, R.E., Smith, W.M., Fast, V.G.: Optical measurements of intramural action potentials in isolated porcine hearts using optrodes. Heart Rhythm **4**(11), 1430–1436 (2007)
14. Lee, A.W., et al.: A rule-based method for predicting the electrical activation of the heart with cardiac resynchronization therapy from non-invasive clinical data. Med. Image Anal. **57**, 197–213 (2019)
15. Lopez-Perez, A., Sebastian, R., Izquierdo, M., Ruiz, R., Bishop, M., Ferrero, J.M.: Personalized cardiac computational models: from clinical data to simulation of infarct-related ventricular tachycardia. Front. Physiol. **10**, 580 (2019)
16. Mendonca Costa, C., Plank, G., Rinaldi, C.A., Niederer, S.A., Bishop, M.J.: Modeling the electrophysiological properties of the infarct border zone. Front. Physiol. **9**, 356 (2018)
17. Mihalef, V., Mansi, T., Rapaka, S., Passerini, T.: Implementation of a patient-specific cardiac model. In: Artificial Intelligence for Computational Modeling of the Heart, pp. 43–94. Elsevier (2020)
18. Mihalef, V., Passerini, T., Mansi, T.: Multi-scale models of the heart for patient-specific simulations. In: Artificial Intelligence for Computational Modeling of the Heart, pp. 3–42. Elsevier (2020)
19. Mitchell, C.C., Schaeffer, D.G.: A two-current model for the dynamics of cardiac membrane. Bull. Math. Biol. **65**(5), 767–793 (2003)
20. Prakosa, A., et al.: Personalized virtual-heart technology for guiding the ablation of infarct-related ventricular tachycardia. Nat. Biomed. Eng. **2**(10), 732–740 (2018)
21. Rapaka, S., et al.: LBM-EP: Lattice-Boltzmann method for fast cardiac electrophysiology simulation from 3D images. In: Ayache, N., Delingette, H., Golland, P., Mori, K. (eds.) MICCAI 2012. LNCS, vol. 7511, pp. 33–40. Springer, Heidelberg (2012). https://doi.org/10.1007/978-3-642-33418-4_5
22. Santangeli, P., et al.: Comparative effectiveness of antiarrhythmic drugs and catheter ablation for the prevention of recurrent ventricular tachycardia in patients with implantable cardioverter-defibrillators: a systematic review and meta-analysis of randomized controlled trials. Heart Rhythm **13**(7), 1552–1559 (2016)
23. Schmidt, A., et al.: Infarct tissue heterogeneity by magnetic resonance imaging identifies enhanced cardiac arrhythmia susceptibility in patients with left ventricular dysfunction. Circulation **115**(15), 2006–2014 (2007)
24. Tranum-Jensen, J., Wilde, A., Vermeulen, J.T., Janse, M.J.: Morphology of electrophysiologically identified junctions between purkinje fibers and ventricular muscle in rabbit and pig hearts. Circ. Res. **69**(2), 429–437 (1991)
25. Trayanova, N.A., Doshi, A.N., Prakosa, A.: How personalized heart modeling can help treatment of lethal arrhythmias: a focus on ventricular tachycardia ablation strategies in post-infarction patients. Wiley Interdiscip. Rev. Syst. Biol. Med. **12**(3), e1477 (2020)
26. Zettinig, O., et al.: Data-driven estimation of cardiac electrical diffusivity from 12-lead ECG signals. Med. Image Anal. **18**(8), 1361–1376 (2014)